2019 IEEE 16th International Symposium on Biomedical Imaging (ISBI 2019)
Venice, Italy, April 8-11, 2019

NORMAL-BASED INTERPOLATING SUBDIVISION FOR THE GEOMETRIC REPRESENTATION OF DEFORMABLE MODELS

Lucia Romani[⋆] *Anaïs Badoual*[†] *Michael Unser*[†]

[⋆] Dipartimento di Matematica, Alma Mater Studiorum Università di Bologna, Bologna, Italy
[†] Biomedical Imaging Group, École polytechnique fédérale de Lausanne (EPFL), Lausanne, Switzerland

ABSTRACT

We review the normal-based interpolating subdivision scheme proposed in [1]. We show that it allows the user to exactly represent circles/spheres whenever suitable initial data are provided, and we also prove that it enjoys the property of similarity invariance. In summary, we show that it satisfies all the requirements for the construction of a deformable model to be used in the delineation of biomedical images. We then also present experimental examples dealing with the delineation of 2D and 3D biological structures.

Index Terms— Subdivision; circle/sphere reproduction; similarity invariance; deformable model; delineation; biomedical imaging.

1. INTRODUCTION

A subdivision scheme consists in a refinement process that is recursively applied to an initial coarse polyline/polygonal mesh [2, 3]. Once infinitely refined, it provides a continuously-defined curve/surface. Subdivision has become one of the basic geometric tools in computer graphics for representation and modeling [4, 5]. In recent years, a new trend in subdivision has been the use of geometric information, such as normal vectors, to have additional control over the curve/surface shape. A normal-based interpolating subdivision scheme allows one to conveniently generate normal-continuous curves/surfaces starting from a given coarse polyline/triangular mesh having assigned unit normal vectors at all its vertices [1, 6–9]. In the surface case, normal-based subdivision schemes provide an alternative approach to the use of parametric models based on joining triangular surface patches [10]. Their advantage is that, in case of a triangular mesh of arbitrary topology, any surface of arbitrary genus can be effectively represented, and its normal-continuity is automatically guaranteed.

Deformable models are efficient tools for the segmentation of biomedical images [11–13]. They consist in flexible curves/surfaces that are deformed from an initial user-provided configuration toward the boundary of the object to delineate. The deformation can be driven manually, by interactively modifying the parameters of the model, or automatically, by applying suitable energies [14, 15]. Subdivision schemes are ideal methods to describe the curve/surface of a deformable model. In fact, the set of the initial vertices, although discrete, is sufficient to fully describe the continuous limit curve/surface. The deformable model is thus encoded by few parameters. Examples of subdivision schemes for use in the delineation of biological structures can be found in [16–20]. They all deal with scalar subdivision (*i.e.*, iterative methods for the refinement of scalar data) for either curve or surface representation. To the best of our knowledge, there are no proposals of vector subdivision schemes for the geometric representation of deformable models. Overall, the incorporation of normal control in deformable models was actually barely exploited and was recently pioneered by [21] for 2D parametric deformable models. We are not aware of any corresponding work in 3D. Yet, the introduction of adjustable normals in a deformable model has several advantages: first, it provides additional control over the shape, which facilitates the reproduction of sharp corners or circonvolutions, for instance; second, it allows for the design of directional energy functionals.

The goal of this paper is to describe the curve/surface of a deformable model by the normal-continuous limit curve/surface obtained with a normal-based interpolating subdivision scheme. Our approach relies on the univariate/bivariate subdivision scheme in [1] (Sections 2,3). Although it uses only the positions and normals at the vertices of each edge/triangle (exactly like local parametric triangular curved shape C^0 methods [22]), it is capable of ensuring smooth limits. We illustrate its capability of reproducing the unit circle/sphere by means of very few control points and associated unit normal vectors, as well as of obtaining blob-like shapes if applied to an arbitrary convex polygon/polyhedron (Subsections 2.2, 3.1). We prove that it is invariant to similarity transformations, which is a crucial property for a deformable model (Subsection 2.3). Finally, we provide experimental examples dealing with the delineation of 2D and 3D biological structures (Section 4).

2. THE NORMAL-BASED INTERPOLATING CURVE SUBDIVISION SCHEME

Subdivision schemes with the capability of reproducing circles/spheres may be either linear [23, 24] or non-linear [1, 6, 8, 25]. For the first class of schemes, the refinement rules are simply given by linear combinations of vector data (*i.e.*, vectors containing function and derivative values, or points and associated normals) from the previous level, while for the second class they are of non-linear type and usually provided by a geometric construction. However, both kinds of methods are designed such that the initial set of vector data is interpolated. The present proposal relies on the non-linear vector subdivision scheme proposed in [1]. It provides normal-continuous limits and has the advantage to use the same refinement rules (hereinafter summarized) for both curve and surface generation. For this reason we privilege this scheme among the various existing proposals.

2.1. Refinement Rules

We denote by $\{\mathbf{p}_i^0, \mathbf{n}_i^0\}_i$ the set of vector data, made of points and associated unit normal vectors. The refinement rules of the normal-based interpolating subdivision scheme from [1] for generating

A. Badoual and M. Unser are funded by the Swiss National Science Foundation under Grant 200020-162343.

$\{\mathbf{p}_i^{k+1}, \mathbf{n}_i^{k+1}\}_i$ starting from $\{\mathbf{p}_i^k, \mathbf{n}_i^k\}_i$ can be concisely written as

$$\begin{aligned} \mathbf{p}_{2i}^{k+1} &= \mathbf{p}_i^k, \\ \mathbf{n}_{2i}^{k+1} &= \mathbf{n}_i^k, \\ \mathbf{p}_{2i+1}^{k+1} &= \tfrac{1}{2}(\mathbf{p}_i^k + \mathbf{p}_{i+1}^k) + \tfrac{1}{8}(\gamma_0^k \mathbf{t}_i^k - \gamma_1^k \mathbf{t}_{i+1}^k), \\ \mathbf{n}_{2i+1}^{k+1} &= \frac{\mathbf{f}^k \times \mathbf{t}_{2i+1}^{k+1}}{\|\mathbf{f}^k \times \mathbf{t}_{2i+1}^{k+1}\|_2}, \end{aligned} \tag{1}$$

where the vectors $\mathbf{t}_i^k, \mathbf{t}_{i+1}^k, \mathbf{t}_{2i+1}^{k+1}$ and $\mathbf{f}^k$ are obtained from $\{\mathbf{p}_i^k, \mathbf{n}_i^k\}_i$ as follows:

$$\begin{aligned} &\mathbf{e}^k = \mathbf{p}_{i+1}^k - \mathbf{p}_i^k, \\ &\mathbf{f}_i^k = \frac{\mathbf{e}^k \times \mathbf{n}_i^k}{\|\mathbf{e}^k \times \mathbf{n}_i^k\|_2}, \quad \mathbf{f}_{i+1}^k = \frac{\mathbf{e}^k \times \mathbf{n}_{i+1}^k}{\|\mathbf{e}^k \times \mathbf{n}_{i+1}^k\|_2}, \quad \mathbf{f}^k = \frac{\mathbf{f}_i^k + \mathbf{f}_{i+1}^k}{\|\mathbf{f}_i^k + \mathbf{f}_{i+1}^k\|_2}, \\ &\mathbf{t}_i^k = \mathbf{e}^k - (\mathbf{n}_i^k \cdot \mathbf{e}^k)\,\mathbf{n}_i^k, \quad \mathbf{t}_{i+1}^k = \mathbf{e}^k - (\mathbf{n}_{i+1}^k \cdot \mathbf{e}^k)\,\mathbf{n}_{i+1}^k, \\ &\cos(\alpha^k) = \frac{(\mathbf{t}_i^k \cdot \mathbf{e}^k)}{\|\mathbf{t}_i^k\|_2 \, \|\mathbf{e}^k\|_2}, \quad \sin(\alpha^k) = \sqrt{1 - \cos^2(\alpha^k)}, \\ &\cos(\beta^k) = \frac{(\mathbf{t}_{i+1}^k \cdot \mathbf{e}^k)}{\|\mathbf{t}_{i+1}^k\|_2 \, \|\mathbf{e}^k\|_2}, \quad \sin(\beta^k) = \sqrt{1 - \cos^2(\beta^k)}, \\ &\gamma_0^k = \frac{4\sin(\beta^k)}{\cos(\alpha^k)(\cos(\alpha^k)+1)(\sin(\alpha^k)+\sin(\beta^k))}, \\ &\gamma_1^k = \frac{4\sin(\alpha^k)}{\cos(\beta^k)(\cos(\beta^k)+1)(\sin(\alpha^k)+\sin(\beta^k))}, \\ &\mathbf{t}_{2i+1}^{k+1} = \tfrac{3}{2}\mathbf{e}^k - \tfrac{1}{4}(\gamma_0^k \mathbf{t}_i^k + \gamma_1^k \mathbf{t}_{i+1}^k). \end{aligned}$$

The graphical interpretation of the refinement rules in (1) is illustrated in Fig. 1.

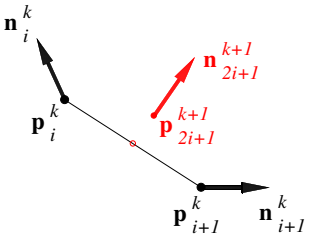

Fig. 1. Graphical illustration of the k-th step of the normal-based interpolating subdivision scheme.

2.2. Reproduction of the Unit Circle

A key property of the subdivision scheme described by (1) is that it reproduces circles. To reproduce the unit circle, we have to start from the inscribed regular n-sided polygon ($n \geq 3$) and its unit normal vectors, *i.e.*, the input data are

$$\mathbf{p}_j^0 = \mathbf{n}_j^0 = \left(\cos\left(\frac{2\pi j}{n}\right), \sin\left(\frac{2\pi j}{n}\right)\right)^T, \quad j = 0, ..., n-1.$$

In Fig. 2 we show the unit circle obtained as limit curve of the normal-based interpolating subdivision scheme when $n = 3, 4$. If we start the refinement with an arbitrary n-sided polygon and some associated unit normal vectors, we get a normal-continuous limit curve with a blob-like shape (see Fig. 3).

2.3. Similarity Invariance

An important requirement for the construction of a deformable model is that the representation model be invariant under similarity transformations. In fact, we are interested in outlining shapes irrespective of their position and orientation. In Proposition 2.1 we show that the normal-based interpolating subdivision scheme in (1) is indeed similarity invariant.

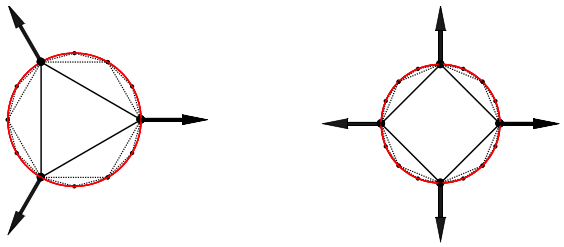

Fig. 2. Unit circles, generated via the normal-based interpolating subdivision scheme, and vertices $\{\mathbf{p}_i^k\}_i$ obtained in levels $k = 1, 2$ when starting from the 3- and 4-sided inscribed regular polygon.

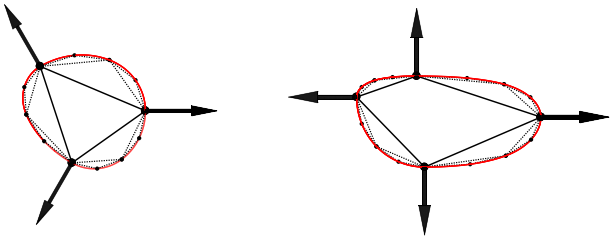

Fig. 3. Blob-like shapes, generated via the normal-based interpolating subdivision scheme, and vertices $\{\mathbf{p}_i^k\}_i$ obtained in levels $k = 1, 2$ when starting from an arbitrary 3- and 4-sided polygon.

Proposition 2.1. *The normal-based interpolating subdivision scheme in* (1) *is invariant under translation, isotropic (or uniform) scaling and rotation. More generally, it is invariant under any similarity transformation identified by a matrix* $\mathbf{M} \in \mathbb{R}^{3\times3}$ *that verifies* $\mathbf{M}^T\mathbf{M} = \sqrt[3]{(det(\mathbf{M}))^2}\mathbf{I}$ *with* $\mathbf{I}$ *the identity matrix of size* 3. *Note that,*

- *if* $\mathbf{M}$ *is a rotation, then* $det(\mathbf{M}) = \pm 1$ *and* $\mathbf{M}^T\mathbf{M} = \mathbf{I}$;
- *if* $\mathbf{M}$ *is an isotropic scaling, then* $\mathbf{M} = m\mathbf{I}$ *and thus* $det(\mathbf{M}) = m^3$ *and* $\mathbf{M}^T\mathbf{M} = m^2\mathbf{I}$.

The proof of Proposition 2.1 is given in Appendix 6.

3. THE NORMAL-BASED INTERPOLATING SURFACE SUBDIVISION SCHEME

The curve subdivision scheme (1) can be extended for surface generation. The idea is to refine each triangle of a given triangular mesh into four subtriangles. By applying recursively this strategy, we generate the limit surface. During the subdivision process, the splitting of each triangle is achieved by applying the curve scheme (1) on each edge of the coarse triangle. We thus ensure that the original triangle vertices and their unit normal vectors are kept, while a new vertex and the associated unit normal vector are defined in correspondence to the midpoint of each triangle edge. By joining together the new vertices, we obtain the refined triangular mesh. The advantage of this method is that the refinement strategy turns out to be very efficient and easy to implement since it uses only local information. Moreover, since all triangles sharing a vertex have the same unit normal vector, normal-continuity of the limit surface comes for free and no proof is needed. Furthermore, if suitable initial data are considered (see Subsection 3.1) the unit sphere can be reproduced.

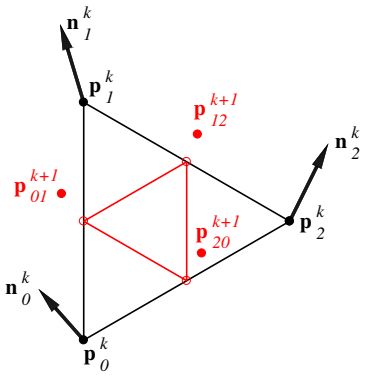

Fig. 4. Graphical illustration of the k-th step of the normal-based interpolating subdivision scheme on a triangular mesh.

3.1. Reproduction of the Unit Sphere

To generate the unit sphere (see Fig. 5), as k approaches infinity, we apply the described subdivision scheme to the tetrahedron of vertices

$$\begin{aligned} \mathbf{p}_0^0 &= \Big(0,0,1\Big)^T, \quad \mathbf{p}_1^0 = \Big(-\sqrt{\tfrac{2}{9}}, -\sqrt{\tfrac{2}{3}}, -\tfrac{1}{3}\Big)^T \\ \mathbf{p}_2^0 &= \Big(-\sqrt{\tfrac{2}{9}}, \sqrt{\tfrac{2}{3}}, -\tfrac{1}{3}\Big)^T, \quad \mathbf{p}_3^0 = \Big(\sqrt{\tfrac{8}{9}}, 0, -\tfrac{1}{3}\Big)^T, \end{aligned}$$

with associated unit normal vectors $\mathbf{n}_j^0 = \frac{\tilde{\mathbf{n}}_j^0}{\|\tilde{\mathbf{n}}_j^0\|_2}$, $j = 0,1,2,3$ where

$$\begin{aligned} \tilde{\mathbf{n}}_0^0 &= \Big(0,0,2\Big)^T, \quad \tilde{\mathbf{n}}_1^0 = \Big(-2\sqrt{\tfrac{2}{9}}, -2\sqrt{\tfrac{2}{3}}, -\tfrac{2}{3}\Big)^T, \\ \tilde{\mathbf{n}}_2^0 &= \Big(-2\sqrt{\tfrac{2}{9}}, 2\sqrt{\tfrac{2}{3}}, -\tfrac{2}{3}\Big)^T, \quad \tilde{\mathbf{n}}_3^0 = \Big(2\sqrt{\tfrac{8}{9}}, 0, -\tfrac{2}{3}\Big)^T. \end{aligned}$$

On the other hand, if we start the refinement with an arbitrary tetrahedron and some associated unit normal vectors, we get a normal-continuous limit surface with a blob-like shape (see Fig. 6).

4. APPLICATION: DELINEATION OF BIOLOGICAL STRUCTURES

We exploit the normal-based interpolating subdivision scheme to efficiently construct 2D and 3D deformable models. Such delineation methods offer the following advantages: i) easy and localized interactions can be achieved by simply modifying the vertices of the initial coarse polyline/triangular mesh; ii) an accurate control over the shape is possible through the normal vectors; iii) directional energy functionals can be designed; iv) the discrete nature of the scheme leads to an easy implementation; v) in the 3D case, the model can handle surfaces of arbitrary topological type.

4.1. Deformable Models

We describe the deformable model by the limit curve/surface of the subdivision scheme. Its shape is entirely encoded by the vertices $\{\mathbf{p}_i^0\}_i$ of the initial coarse polyline/triangular mesh, so called *control points*, and by the associated unit normal vectors $\{\mathbf{n}_i^0\}_i$. The parameters of the model are thus the control points and the unit normal vectors. To attract the curve/surface towards the structure of interest in the image, we locally adjust the control points. This can be done either manually or automatically by minimizing a suitable energy functional [21].

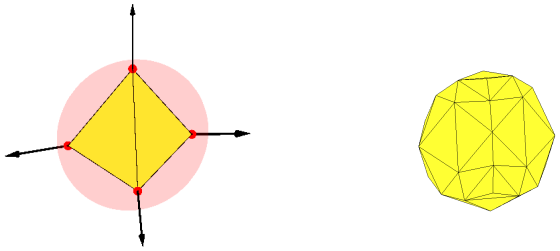

(a) $k = 0$ (b) $k = 2$

(c) $k = 3$ (d) $k = 7$

Fig. 5. Vertices generated via the normal-based interpolating subdivision scheme in levels $k = 2,3,7$ (b,c,d) when starting from the regular tetrahedron with associated unit normal vectors (a).

A good 2D/3D deformable model must fulfill two main requirements. First, to efficiently detect blob-like objects, it must reproduce circles/spheres. Second, it must depend on a small number of parameters to limit the complexity of the deformation and improve robustness. This is especially true in 3D: in order to have few control points to manipulate, and as the number of vertices increases geometrically at each subdivision step, we want a simple shape as initial coarse triangular mesh. Since we focus our attention on the construction of deformable models for the characterization of closed biomedical structures, we choose as initial mesh a 2-manifold triangular mesh with genus 0. In particular, among the Platonic solids having triangular faces and the lowest possible number of vertices, we choose the tetrahedron as initial coarse mesh for the bivariate subdivision scheme.

4.2. Experimental Results

We illustrate the use of this deformable model on four bioimages (see Fig. 7). For those examples the deformation was performed manually. The model is able to delineate structures with blob-like shape (sphere-like shape, respectively) (see Fig. 7 (b) and (d)), as well as more complex shapes with circonvolutions or rapid changes of orientation (see Fig. 7 (a) and (c)). In fact, the additional information and control of the normals make the model more robust to circonvolutions than the traditional deformable models [26]. The average time to manually delineate each structure was less than 30 seconds, starting from an initialization close to the object to segment.

5. CONCLUSION

We have shown that the normal-based interpolating subdivision scheme in [1] possesses all the requirements to provide a computationally efficient representation of curves and surfaces to be used in the construction of 2D and 3D deformable models. We have illustrated the benefits of a deformable model with normal control in the delineation of biological structures with circonvolutions or rapid changes of orientation.

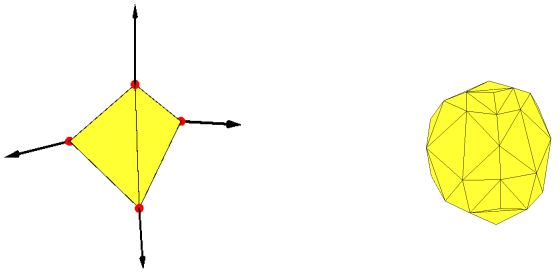

(a) $k=0$ (b) $k=2$

(c) $k=3$ (d) $k=7$

Fig. 6. Vertices generated via the normal-based interpolating subdivision scheme in levels $k=2,3,7$ (b,c,d) when starting from an arbitrary tetrahedron and some associated unit normal vectors (a).

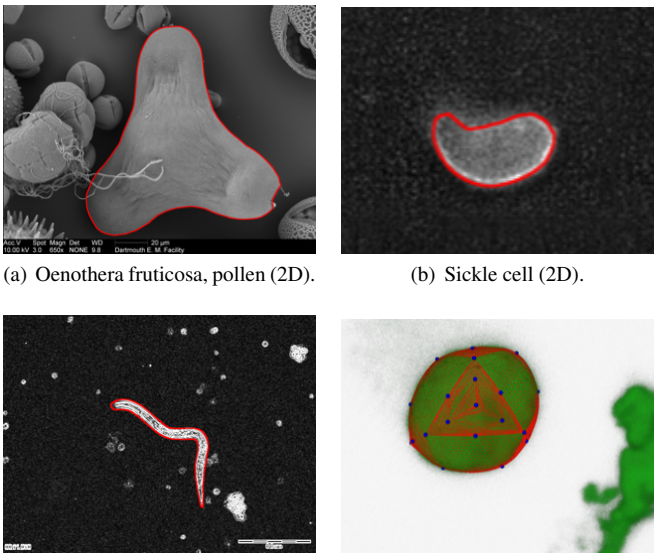

(a) Oenothera fruticosa, pollen (2D). (b) Sickle cell (2D).

(c) *C. elegans* (2D). (d) Nuclei (3D).

Fig. 7. Delineation of biomedical structures in 2D-3D microscopy images. (a) Oenothera fruticosa, pollen, in a 2D image, source: Louisa Howard (2012), doi:10.7295/W9CIL40334; (b) Sickle cell in a 2D image; (c) *C. elegans* in a 2D image; (d) Nuclei in a volume. The blue dots are the control points of the 3D deformable model.

6. APPENDIX: PROOF OF PROPOSITION 2.1

We first prove the invariance by *translation*. Let $\mathbf{s}\in\mathbb{R}^3$ be a translation vector applied to the kth level set of points, namely let $\hat{\mathbf{p}}_i^k = \mathbf{p}_i^k+\mathbf{s}$ for all i. The normal vectors $\mathbf{n}_i^k$ are not affected by this transformation, *i.e.*, $\hat{\mathbf{n}}_i^k=\mathbf{n}_i^k$ for all i. In the following we show that the refinement rules (1) yield the refined set of points $\hat{\mathbf{p}}_i^{k+1}=\mathbf{p}_i^{k+1}+\mathbf{s}$ and the associated normals $\hat{\mathbf{n}}_i^{k+1}=\mathbf{n}_i^{k+1}$.

First of all, we easily show that $\hat{\mathbf{e}}^k=\hat{\mathbf{p}}_{i+1}^k-\hat{\mathbf{p}}_i^k=\mathbf{e}^k$. As $\mathbf{f}_i^k$ and $\mathbf{t}_i^k$ only depend on $\mathbf{n}_i^k$ and $\mathbf{e}^k$ for all i, we deduce that they remain unchanged by translation. The same applies to $\mathbf{f}^k$, γ_0^k and γ_1^k. We can thus show that

$$\hat{\mathbf{t}}_{2i+1}^{k+1} = \tfrac{3}{2}\hat{\mathbf{e}}^k-\tfrac{1}{4}(\gamma_0^k\mathbf{t}_i^k+\gamma_1^k\mathbf{t}_{i+1}^k)=\mathbf{t}_{2i+1}^{k+1},$$

and

$$\begin{aligned}
\hat{\mathbf{p}}_{2i}^{k+1} &= \hat{\mathbf{p}}_i^k=\mathbf{p}_i^k+\mathbf{s}=\mathbf{p}_{2i}^{k+1}+\mathbf{s},\\
\hat{\mathbf{p}}_{2i+1}^{k+1} &= \tfrac{1}{2}\Big((\mathbf{p}_i^k+\mathbf{s})+(\mathbf{p}_{i+1}^k+\mathbf{s})\Big)+\tfrac{1}{8}(\gamma_0^k\mathbf{t}_i^k-\gamma_1^k\mathbf{t}_{i+1}^k)\\
&= \mathbf{p}_{2i+1}^{k+1}+\mathbf{s},\\
\hat{\mathbf{n}}_{2i}^{k+1} &= \hat{\mathbf{n}}_i^k=\mathbf{n}_i^k=\mathbf{n}_{2i}^{k+1},\\
\hat{\mathbf{n}}_{2i+1}^{k+1} &= \frac{\hat{\mathbf{f}}^k\times\hat{\mathbf{t}}_{2i+1}^{k+1}}{\|\hat{\mathbf{f}}^k\times\hat{\mathbf{t}}_{2i+1}^{k+1}\|_2}=\frac{\mathbf{f}^k\times\mathbf{t}_{2i+1}^{k+1}}{\|\mathbf{f}^k\times\mathbf{t}_{2i+1}^{k+1}\|_2}=\mathbf{n}_{2i+1}^{k+1},
\end{aligned}$$

which correspond to the condition of translation invariance.

To show invariance under *isotropic (or uniform) scaling and rotation*, we first recall the following results. Let $\mathbf{a},\mathbf{b}\in\mathbb{R}^3$ and $\mathbf{M}\in\mathbb{R}^{3\times3}$ such that $\mathbf{M}^T\mathbf{M}=\sqrt[3]{(det(\mathbf{M}))^2}\mathbf{I}$. Then, we have that

$$(\mathbf{Ma})\cdot(\mathbf{Mb})=\sqrt[3]{(det(\mathbf{M}))^2}\,(\mathbf{a}\cdot\mathbf{b}) \tag{2}$$

and

$$(\mathbf{Ma})\times(\mathbf{Mb})=\sqrt[3]{det(\mathbf{M})}\,\mathbf{M}\,(\mathbf{a}\times\mathbf{b}). \tag{3}$$

In the case of isotropic (or uniform) scaling and rotation, the refinement rules (1) are applied to $\hat{\mathbf{p}}_i^k=\mathbf{M}\mathbf{p}_i^k$ and $\hat{\mathbf{n}}_i^k=\frac{\mathbf{M}\mathbf{n}_i^k}{\|\mathbf{M}\mathbf{n}_i^k\|_2}=\frac{\mathbf{M}\mathbf{n}_i^k}{\sqrt[3]{det(\mathbf{M})}}$. In light of (2) and (3) we have

$$\begin{aligned}
\hat{\mathbf{e}}^k &= \hat{\mathbf{p}}_{i+1}^k-\hat{\mathbf{p}}_i^k=\mathbf{M}\mathbf{e}^k,\\
\hat{\mathbf{f}}_i^k &= \frac{\hat{\mathbf{e}}^k\times\hat{\mathbf{n}}_i^k}{\|\hat{\mathbf{e}}^k\times\hat{\mathbf{n}}_i^k\|_2}=\frac{\mathbf{M}\mathbf{e}^k\times\mathbf{M}\mathbf{n}_i^k}{\|\mathbf{M}\mathbf{e}^k\times\mathbf{M}\mathbf{n}_i^k\|_2}=\frac{\mathbf{M}\mathbf{f}_i^k}{\sqrt[3]{det(\mathbf{M})}},\\
\hat{\mathbf{f}}^k &= \frac{\hat{\mathbf{f}}_i^k+\hat{\mathbf{f}}_{i+1}^k}{\|\hat{\mathbf{f}}_i^k+\hat{\mathbf{f}}_{i+1}^k\|_2}=\frac{\mathbf{M}(\mathbf{f}_i^k+\mathbf{f}_{i+1}^k)}{\|\mathbf{M}(\mathbf{f}_i^k+\mathbf{f}_{i+1}^k)\|_2}=\frac{\mathbf{M}\mathbf{f}^k}{\sqrt[3]{det(\mathbf{M})}},\\
\hat{\mathbf{t}}_i^k &= \hat{\mathbf{e}}^k-(\hat{\mathbf{n}}_i^k\cdot\hat{\mathbf{e}}^k)\,\hat{\mathbf{n}}_i^k\\
&= \mathbf{M}\mathbf{e}^k-\Big(\tfrac{1}{\sqrt[3]{det(\mathbf{M})}}(\mathbf{M}\mathbf{n}_i^k)\cdot(\mathbf{M}\mathbf{e}^k)\Big)\,\tfrac{\mathbf{M}\mathbf{n}_i^k}{\sqrt[3]{det(\mathbf{M})}}\\
&= \mathbf{M}\mathbf{t}_i^k,\\
\widehat{\cos(\alpha^k)} &= \frac{\hat{\mathbf{t}}_i^k\cdot\hat{\mathbf{e}}^k}{\|\hat{\mathbf{t}}_i^k\|_2\,\|\hat{\mathbf{e}}^k\|_2}=\frac{(\mathbf{M}\mathbf{t}_i^k)\cdot(\mathbf{M}\mathbf{e}^k)}{\|\mathbf{M}\mathbf{t}_i^k\|_2\,\|\mathbf{M}\mathbf{e}^k\|_2}=\cos(\alpha^k).
\end{aligned}$$

Hence, $\cos(\alpha^k)$ is not altered by the transformation $\mathbf{M}$, and thus neither γ_0^k nor γ_1^k are. At the $(k+1)$th level we thus get

$$\hat{\mathbf{t}}_{2i+1}^{k+1} = \tfrac{3}{2}\hat{\mathbf{e}}^k-\tfrac{1}{4}(\gamma_0^k\hat{\mathbf{t}}_i^k+\gamma_1^k\hat{\mathbf{t}}_{i+1}^k)=\mathbf{M}\mathbf{t}_{2i+1}^{k+1},$$

and

$$\begin{aligned}
\hat{\mathbf{p}}_{2i}^{k+1} &= \hat{\mathbf{p}}_i^k=\mathbf{M}\mathbf{p}_i^k=\mathbf{M}\mathbf{p}_{2i}^{k+1},\\
\hat{\mathbf{p}}_{2i+1}^{k+1} &= \tfrac{1}{2}(\hat{\mathbf{p}}_i^k+\hat{\mathbf{p}}_{i+1}^k)+\tfrac{1}{8}(\gamma_0^k\hat{\mathbf{t}}_i^k-\gamma_1^k\hat{\mathbf{t}}_{i+1}^k)=\mathbf{M}\mathbf{p}_{2i+1}^{k+1}\\
\hat{\mathbf{n}}_{2i}^{k+1} &= \hat{\mathbf{n}}_i^k=\frac{\mathbf{M}\mathbf{n}_i^k}{\sqrt[3]{det(\mathbf{M})}}=\frac{\mathbf{M}\mathbf{n}_{2i}^{k+1}}{\sqrt[3]{det(\mathbf{M})}},\\
\hat{\mathbf{n}}_{2i+1}^{k+1} &= \frac{\hat{\mathbf{f}}^k\times\hat{\mathbf{t}}_{2i+1}^{k+1}}{\|\hat{\mathbf{f}}^k\times\hat{\mathbf{t}}_{2i+1}^{k+1}\|_2}=\frac{\mathbf{M}\mathbf{f}^k\times\mathbf{M}\mathbf{t}_{2i+1}^{k+1}}{\|\mathbf{M}\mathbf{f}^k\times\mathbf{M}\mathbf{t}_{2i+1}^{k+1}\|_2}=\frac{\mathbf{M}\mathbf{n}_{2i+1}^{k+1}}{\sqrt[3]{det(\mathbf{M})}}.
\end{aligned}$$

Note that $\|\mathbf{M}\mathbf{n}_{2i+j}^{k+1}\|_2=\sqrt[3]{det(\mathbf{M})}\|\mathbf{n}_{2i+j}^{k+1}\|_2=\sqrt[3]{det(\mathbf{M})}$, for $j=0,1$. Then $\hat{\mathbf{n}}_{2i+j}^{k+1}$, $j=0,1$, are still unit normal vectors, which concludes the proof.

7. REFERENCES

[1] M. Aihua, L. Jie, C. Jun, and L. Guiqing, "A new fast normal-based interpolating subdivision scheme by cubic Bézier curves," *The Visual Computer*, vol. 32, no. 9, pp. 1085–1095, 2016.

[2] N. Dyn, "Subdivision schemes in CAGD," *Advances in Numerical Analysis*, vol. 2, pp. 36–104, 1992.

[3] A. Myles, K. Karciauskas, and J. Peters, "Extending Catmull-Clark subdivision and PCCM with polar structures," in *IEEE Proceedings of the 15th Pacific Conference on Computer Graphics and Applications*, Washington, DC, USA, 2007, pp. 313–320.

[4] T. DeRose, M. Kass, and T. Truong, "Subdivision surfaces in character animation," in *Proceedings of the 25th annual conference on Computer Graphics and interactive techniques*, New York, NY, USA, 1998, ACM, pp. 85–94.

[5] A. Lee, H. Moreton, and H. Hoppe, "Displaced subdivision surfaces," in *Proceedings of the 27th annual conference on Computer graphics and interactive techniques*, New York, NY, USA, 2000, ACM Press/Addison-Wesley Publishing Co., pp. 85–94.

[6] S. Karbacher, S. Seeger, and G. Häusler, "Refining triangle meshes by non-linear subdivision," in *Proceedings of International Conference on 3-D Digital Imaging and Modeling, 3DIM*, 2001, pp. 270–277.

[7] X. Yang, "Normal based subdivision scheme for curve design," *Computer Aided Geometric Design*, vol. 23, no. 3, pp. 243–260, 2006.

[8] P. Chalmovianský and B. Jüttler, "A non-linear circle-preserving subdivision scheme," *Advances in Computational Mathematics*, vol. 27, no. 4, pp. 375–400, 2007.

[9] E. Lipovetsky and N. Dyn, "A weighted binary average of point-normal pairs with application to subdivision schemes," *Computer Aided Geometric Design*, vol. 48, pp. 36–48, 2016.

[10] M. Boschiroli, C. Fünfzig, L. Romani, and G. Albrecht, "G^1 rational blend interpolatory schemes: A comparative study," *Graphical Models*, vol. 74, no. 1, pp. 29 – 49, 2012.

[11] R. Delgado-Gonzalo, V. Uhlmann, D. Schmitter, and M. Unser, "Snakes on a plane: A perfect snap for bioimage analysis," *IEEE Signal Processing Magazine*, vol. 32, no. 1, pp. 41–48, 2015.

[12] B. De Leener, S. Kadoury, and J. Cohen-Adad, "Robust, accurate and fast automatic segmentation of the spinal cord," *NeuroImage*, vol. 98, pp. 528–536, 2014.

[13] A. Dufour, R. Thibeaux, E. Labruyere, N. Guillen, and J.-C. Olivo-Marin, "3-D Active meshes: Fast discrete deformable models for cell tracking in 3-D time-lapse microscopy," *IEEE Transactions on Image Processing*, vol. 20, no. 7, pp. 1925–1937, 2011.

[14] G. Székely, A. Kelemen, C. Brechbhler, and G. Gerig, "Segmentation of 2D and 3D objects from MRI volume data using constrained elastic deformations of flexible fourier contour and surface models," *Medical Image Analysis*, vol. 1, no. 1, pp. 19–24, 1996.

[15] M. Jacob, T. Blu, and M. Unser, "Efficient energies and algorithms for parametric snakes," *IEEE Transactions on Image Processing*, vol. 13, no. 9, pp. 1231–1244, 2004.

[16] A. Badoual, D. Schmitter, V. Uhlmann, and M. Unser, "Multiresolution subdivision snakes," *IEEE Transactions on Image Processing*, vol. 26, no. 3, pp. 1188–1201, 2017.

[17] J. Hug, C. Brechbühler, and G. Székely, "Tamed snake: A particle system for robust semi-automatic segmentation," in *International Conference on Medical Image Computing and Computer-Assisted Intervention*, 1999, vol. 1679, pp. 106–115.

[18] P.H. Kitslaar, R. Vant Klooster, M. Staring, B.P.F. Lelieveldt, and R.J. Van Der Geest, "Segmentation of branching vascular structures using adaptive subdivision surface fitting," in *Progress in Biomedical Optics and Imaging - Proceedings of SPIE*, Orlando, Florida, United States, 2015, International Society for Optics and Photonics, vol. 9413, p. 94133Z.

[19] F. Orderud and S. I. Rabben, "Real-time 3D segmentation of the left ventricle using deformable subdivision surfaces," in *26th IEEE Conference on Computer Vision and Pattern Recognition*, 2008, pp. 1–8.

[20] A. Badoual, P. Novara, L. Romani, D. Schmitter, and M. Unser, "A non-stationary subdivision scheme for the construction of deformable models with sphere-like topology," *Graphical Models*, vol. 94, pp. 38–51, 2017.

[21] V. Uhlmann, R. Delgado-Gonzalo, C. Conti, L. Romani, and M. Unser, "Exponential Hermite splines for the analysis of biomedical images," in *ICASSP, IEEE International Conference on Acoustics, Speech and Signal Processing - Proceedings*, 2014, pp. 1631–1634.

[22] M. Boschiroli, C. Fünfzig, L. Romani, and G. Albrecht, "A comparison of local parametric C^0 Bézier interpolants for triangular meshes," *Computers & Graphics*, vol. 35, no. 1, pp. 20 – 34, 2011.

[23] C. Conti, J.-L. Merrien, and L. Romani, "Dual Hermite subdivision schemes of de Rham-type," *BIT Numerical Mathematics*, vol. 54, no. 4, pp. 955–977, 2014.

[24] C. Conti, L. Romani, and M. Unser, "Ellipse-preserving Hermite interpolation and subdivision," *Journal of Mathematical Analysis and Applications*, vol. 426, no. 1, pp. 211–227, 2015.

[25] L. Romani, "A circle-preserving C^2 Hermite interpolatory subdivision scheme with tension control," *Computer Aided Geometric Design*, vol. 27, no. 1, pp. 36–47, 2010.

[26] R. Delgado-Gonzalo, P. Thévenaz, C. S. Seelamantula, and M. Unser, "Snakes with an ellipse-reproducing property," *IEEE Transactions on Image Processing*, vol. 21, no. 3, pp. 1258–1271, 2012.